Ferroelectric Liquid-Crystal-Based LiDAR Technology and 3D Depth-Mapping Technique

Yue-Chu Cheng, Vigneshwaran Swaminathan*, Hoi-Sing Kwok*, Abhishek Kumar Srivastava**

***State Key Laboratory of Advanced Displays and Optoelectronics Technologies, Department of Electronic and Computer Engineering, The Hong Kong University of Science and Technology, Hong Kong S.A.R., China**

Abstract

This study presents a LiDAR system based on ferroelectric liquid crystal technology, integrated with advanced depth mapping and 3D reconstruction algorithms. The system utilizes fast liquid crystal gratings for light modulation, enabling a switchable field of view up to 72 degrees. The generated point cloud is processed through a depth mapping algorithm, which is based on a data pre-training method to convert pixel-based data into real-world distances.

Author Keywords

Liquid crystal; LiDAR; Depth Mapping; 3D Reconstruction

1. Introduction

LiDAR (Light Detection and Ranging) is a key technology used in various fields, including autonomous vehicles, robotics, and environmental monitoring, due to its ability to capture 3D spatial structures with precision[1]. However, traditional LiDAR systems face challenges such as slow scanning speed, limited field of view (FoV), low resolution, and high costs, which hinder their scalability and suitability for next-generation applications[2].

Recent advancements in LiDAR technology have introduced systems addressing traditional limitations. Mechanical LiDAR, known for its maturity and high resolution, uses rotating components but is limited by wear, slow scanning, and bulkiness[3]. Solid-state LiDAR, which removes mechanical parts, offers faster and more robust solutions. MEMS-based LiDAR is compact and fast but sacrifices field of view (FoV) and resolution, while flash LiDAR captures entire scenes instantly but faces range and resolution trade-offs[4]. A more recent innovation involves optical phased arrays (OPAs), which enable precise, electronic beam steering without moving parts[5]. While OPAs offer promise for high-speed and wide-angle scanning, their scalability is limited by complex fabrication processes and challenges in achieving high efficiency across large arrays.

Against this backdrop, liquid crystal (LC) technology has emerged as a transformative solution for LiDAR systems. By leveraging the electrically tunable optical properties of LC materials, these systems can achieve fast and precise beam steering, light modulation, and diffraction control. Liquid crystal-based LiDAR systems offer unique advantages, including wide and switchable FoV, low driving voltage, compact design, and high mechanical stability[6].

In this work, we explore the integration of liquid crystal technology with LiDAR systems to overcome the limitations of conventional approaches. By combining fast liquid crystal gratings with advanced depth mapping and 3D reconstruction algorithms, we demonstrate a system capable of achieving enhanced LiDAR scanning and 3D reconstruction performance in terms of speed, FoV, and accuracy.

2. Methodology and experiments

The schematic of the liquid crystal-based LiDAR and 3D reconstruction algorithm is shown in Figure 1.

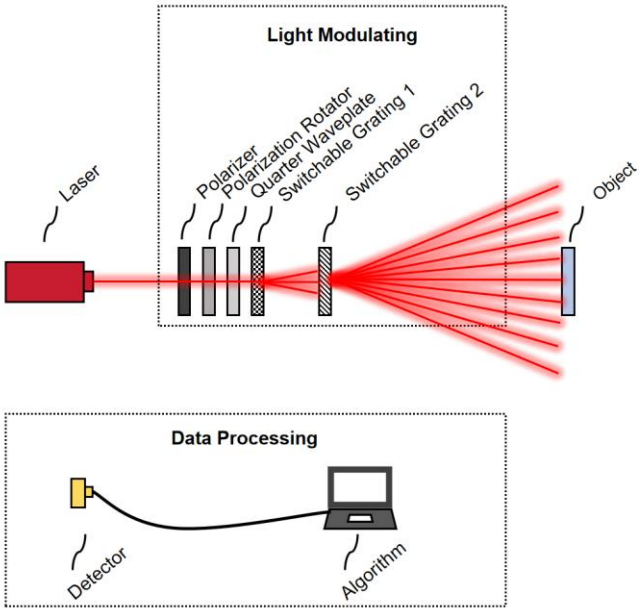

Fig. 1. Schematic of the liquid crystal-based LiDAR and 3D reconstruction system.

The system is composed of two primary components: the beam modulation module and the data processing module. The beam modulation module consists of an electrically switchable polarization state rotator and a set of electrically switchable gratings, which collectively realize beam modulation and deflection. The data processing module not only extracts depth information but also reconstructs 3D models, relying on self-developed algorithms.

ISSN 0097-996X/25/5602-1183-$1.00 © 2025

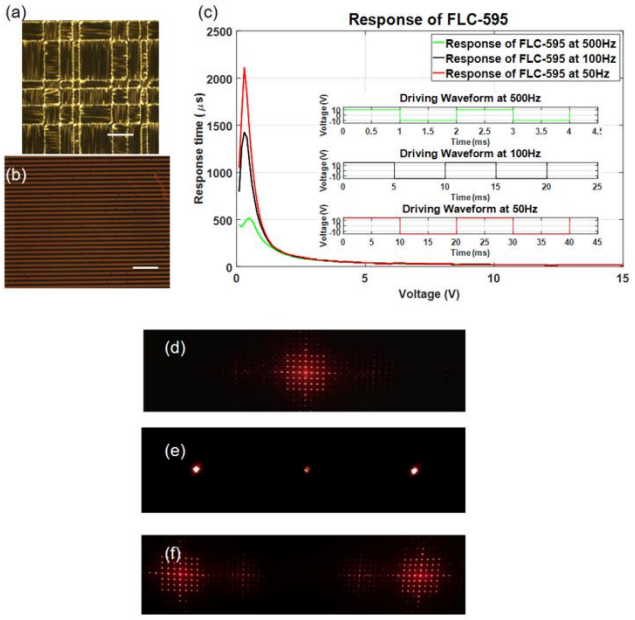

Fig. 2. Beam steering components and effects. (a) Microscopic image of Dammann grating (scale bar: 100 μm), (b) Microscopic image of polarization grating (scale bar: 50 μm), (c) Electro-optical response of ferroelectric liquid crystal, (d) Beam steering effect: Dammann grating ON, polarization grating OFF, (e) Beam steering effect: Dammann grating OFF, polarization grating ON, (f) Beam steering effect: Dammann grating ON, polarization grating ON.

Specifically, the key components of the beam modulation module and the corresponding beam modulation results are illustrated in Figure 2. Figure 2(a) presents a micrograph of the ferroelectric liquid crystal Dammann grating (FLCDG) under polarized light. Dammann gratings (DGs) are binary phase (0, π) gratings specifically designed to create uniform diffraction patterns[7]. By leveraging Fourier optics, the DG pattern ensures precise light division, splitting the incident beam into a uniform 7x7 array of equidistant spots. Each diffracted spot exhibits equal intensity, which is critical for maintaining consistent optical energy distribution in the beam steering process. The grating pattern is fabricated within the liquid crystal cell using photoalignment techniques, and the liquid crystal cell is filled with ferroelectric liquid crystal (FLC) material, known for its fast switching properties[8]. Figure 2(c) showcases the electro-optical characteristics of the FLC material. When a 500 Hz square wave is applied to the FLC cell with a driving voltage of 5V, the response time is approximately 50 μs, demonstrating a fast switching speed.

The liquid crystal polarization grating (LCPG) array is used as a field-of-view extender. Figure 2(b) shows a micrograph of the LCPG under a polarized microscope. Through modulation of the incident light's polarization state using a polarization rotator, combined with the serial connection of multiple electrically switchable LCPG stages, the LCPG array is capable of deflecting the light beam to various angles. This configuration allows for a field-of-view (FoV) expansion of approximately 72 degrees.

The overall beam steering performance of the system is illustrated in Figures 2(d) to 2(f). Figure 2(d) demonstrates the beam pattern when the Dammann grating is activated while the polarization grating is deactivated, resulting in precisely defined diffraction patterns, optimized for static beam projection. Figure 2(e) highlights the effect of activating the polarization grating while deactivating the Dammann grating, leading to polarization-driven beam deflection with enhanced directionality. Finally, Figure 2(f) illustrates the combined activation of both gratings, achieving dynamic and wide-angle beam steering, ideal for scenarios requiring high adaptability and precision. This dual-grating configuration eliminates mechanical moving parts, enhancing system reliability and reducing maintenance costs compared to traditional beam steering solutions such as MEMS-based systems. The results validate the system's capability for fast-switchable beam control.

After fabricating the LiDAR optical modulation components, the system is capable of projecting a point cloud onto an object. The subsequent task involves extracting depth information from this point cloud to create an accurate depth map. For this purpose, we developed a simple yet effective algorithm based on scale conversion and image processing. This algorithm requires only a single camera for data acquisition, making it highly accessible and cost-effective. The flowchart and results of this depth-mapping process are illustrated in Figure 3.

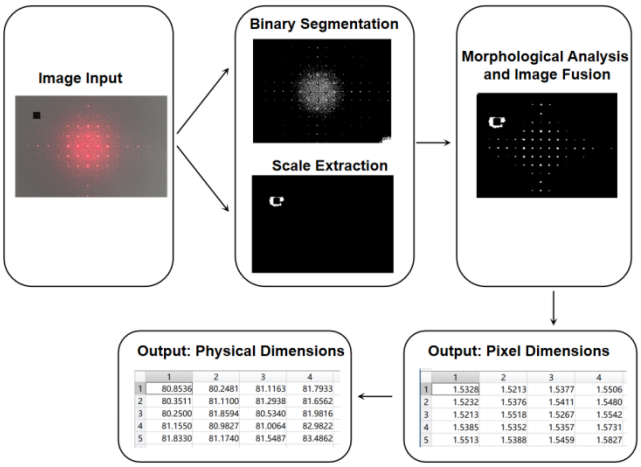

Fig. 3. Flowchart and results of the depth-mapping algorithm based on scale conversion and image processing.

Once the input image is captured, the algorithm applies a series of image processing steps, including thresholding, binary segmentation, and morphological operations, to refine the data. The next stage involves identifying the centers of the light spots and constraining them to align along a single horizontal or vertical line. This step ensures precise extraction of the spot coordinates in pixel dimensions while effectively suppressing interference from stray light sources. To provide a reference for mapping physical dimensions to pixel dimensions, a 1x1 cm square is pre-marked on the detection surface. This reference scale is crucial for establishing accurate depth mapping, as it allows the algorithm to convert physical dimensions into pixel dimensions. Once this mapping is complete, the algorithm generates the depth information of the detected surface in real-world units.

However, one drawback of this method is its dependency on the pre-marked scale square, which limits its practicality in certain scenarios. To address this, we have developed an improved algorithm that eliminates the requirement for a scale reference in

the image. In the improved algorithm, we have developed a data pre-training-based algorithm for depth mapping and 3D reconstruction. The goal is to establish a relationship between the camera's detected image pixel (d) and the real-world distance (D) of the light spots, enabling more efficient mapping of the objects. The algorithm begins by capturing photos of a reference object—a 1 cm long line segment—at various distances, which serves as a calibration standard. By measuring how many pixels correspond to the 1 cm reference, we establish a scaling factor. Next, images of the light spots, which are objects of interest, are taken from the same distances. The spacing between the neighboring light spots is then measured in pixels. By comparing this pixel distance with the known pixel measurement of the reference, we calculate a coefficient that links the pixel-based data to real-world distances. Using this coefficient, we can convert the pixel distances of the light spots into real-world measurements, thereby achieving precise depth mapping and 3D reconstruction of the detected objects.

3. Results

Based on the above discussion, we ultimately optimized the 3D reconstruction method by employing a data pre-training approach. The model training process is illustrated in Figure 4(a). After completing the training phase, the system integrates the image processing methods from the previous Method 1 to directly process test images.

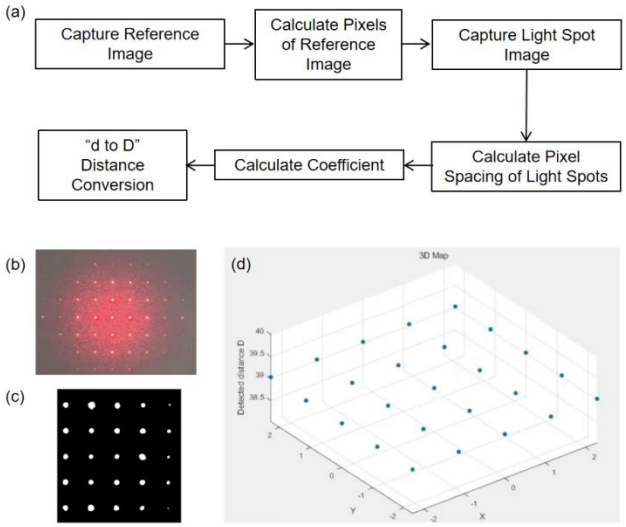

Fig. 4. (a) Flowchart of 3D reconstruction algorithm. (b) Captured image of projected cloud points with liquid crystal beam modulation system. (c) Processed image. (d) 3D reconstruction result of real-world physical dimensions.

Figures 4(b) to 4(d) illustrate the complete workflow, starting from projecting cloud points using the liquid cystal beam modulation system mentioned earlier, to capturing the input image, and finally generating the 3D model. Once the image is captured and input into the system, the algorithm processes the data automatically. It extracts the light spot patterns through post-processing, calculates the pixel dimensions, and maps them to real-world physical dimensions, ultimately producing the reconstructed 3D map.

4. Conclusion and future work

The proposed liquid crystal-based LiDAR system demonstrates advancements in depth mapping and 3D reconstruction through the integration of switchable optical gratings and advanced data processing algorithms. The system successfully bridges the gap between pixel-based measurements and real-world dimensions, providing a cost-effective, and scalable solution for various applications. The adoption of a data pre-training method for depth mapping eliminates the dependency on physical scale markers, enhancing the system's usability and adaptability for real-world scenarios.

Despite these achievements, some limitations remain. The accuracy of the depth mapping and 3D reconstruction heavily relies on the quality of the training dataset and the precision of the light spot detection process. Future improvements could focus on developing more sophisticated algorithms capable of mitigating the effects of such factors.

5. Acknowledgments

This research is supported by the State Key Laboratory of Advanced Displays and Optoelectronics Technologies (HKUST).

6. References

1. Raj, Thinal, et al. "A survey on LiDAR scanning mechanisms." Electronics 9.5 (2020): 741.
2. Roriz, Ricardo, Jorge Cabral, and Tiago Gomes. "Automotive LiDAR technology: A survey." IEEE Transactions on Intelligent Transportation Systems 23.7 (2021): 6282-6297.
3. Li, You, and Javier Ibanez-Guzman. "Lidar for autonomous driving: The principles, challenges, and trends for automotive lidar and perception systems." IEEE Signal Processing Magazine 37.4 (2020): 50-61.
4. Royo, Santiago, and Maria Ballesta-Garcia. "An overview of lidar imaging systems for autonomous vehicles." Applied sciences 9.19 (2019): 4093.
5. Hsu, Ching-Pai, et al. "A review and perspective on optical phased array for automotive LiDAR." IEEE Journal of Selected Topics in Quantum Electronics 27.1 (2020): 1-16.
6. Yuan, Zheng-Nan, et al. "Fast LiDAR systems based on ferroelectric liquid crystal Dammann grating." Liquid Crystals 48.10 (2021): 1402-1416.
7. Ge, Shi-Jun, et al. "Optical array generator based on blue phase liquid crystal Dammann grating." Optical Materials Express 6.4 (2016): 1087-1092.
8. Srivastava, Abhishek Kumar, Vladimir G. Chigrinov, and Hoi-Sing Kwok. "Electrically suppressed helix ferroelectric liquid crystals for modern displays." Journal of the Society for Information Display 23.4 (2015): 176-181.